DOI: 10.1002/chem.200801689

Neutral Nickel(II) and Copper(II) Tetraazamacrocyclic Complexes as Molecular Rods Attached to Gold Electrodes

Urszula E. Wawrzyniak,[a] Mateusz Woźny,[b] Jarosław Kowalski,[b] Sławomir Domagała,[a] Elwira Maicka,[a] Renata Bilewicz,*[a] Krzysztof Woźniak,*[a] and Bohdan Korybut-Daszkiewicz*[b]

Abstract: New dithiolated derivatives of neutral Cu^{II} and Ni^{II} tetraazamacrocyclic complexes have been synthesized and characterized by spectroscopic and diffractional methods. These rod-shaped molecules were assembled in monocomponent and mixed monolayers on gold electrodes. In the mixed monolayers, the active molecules were embedded in a hexanethiol matrix. The dithiolated complexes are oriented perpendicularly to the electrode, and reveal faster kinetics of electron transfer than those assembled in a single-component monolayer. They appear as protrusions, which are easily addressed by using the STM method. In the presence of a suitable electron acceptor in the solution, the donor properties of the anchored Cu complex were weakened, which revealed donor–acceptor interactions with the monolayer. The peak position in the voltammogram indicates a stronger interaction of the solution-based acceptor with the reduced Cu^{II} form than with the Cu^{III} complex. This suggests the possibility of switching the association on or off by applying an appropriate potential.

Keywords: copper · macrocyclic complexes · monolayers · nickel · self-assembly

Introduction

Stimuli-responsive supramolecular assemblies on solid supports would be useful components of molecular machines, which are able to perform tailored mechanical tasks.[1, 2] A collective operation of a monolayer of molecular shuttles may power macroscopic transport, as reported by Berna et al.[3] Millimetre-scale movement was achieved by Brownian motion of stimuli-responsive rotaxanes, simply by changing the surface tension. Electrochemically switchable wettability is also described in the work of Willner et al on benzoquinone monolayer-functionalized electrodes.[4] The same group has reported a molecular switch based on paraquate cyclophane.[5] Upon application of an appropriate potential, the cyclophane unit is reduced, which decreases its π–π interactions with the rotaxane thread and moves this unit towards the negatively charged electrode. The most common rotaxanes immobilized on conductive surfaces are based on cyclophane rings and tetrathiafulvalene units in the thread.[1,6,7] In all of the above examples radicals are produced as a result of electrode processes; this may generate chemical instability at the longer timescales needed in practical devices. To avoid the above difficulty, we rely on using macrocyclic transition-metal complexes as the redox-active sites.[8,9] Sauvage and co-workers have demonstrated that electrochemical reduction of a pentacoordinated Cu species results in pirouetting of the macrocycle around the thread. However, a similar system immobilized on an electrode surface did not show any motion.[1,10,11]

In previous work,[12] we described the redox properties of a neutral tetraazamacrocyclic complex **5·Ni** in solution and demonstrated that it can be anchored to the gold surface by means of thiol groups.[13] In our systems, no chemical reactions around the metal ion center are involved and no changes in the coordination number takes place. Upon oxidation or reduction only π–π interactions are affected.[9] Herein, we describe two neutral π-donor tetraazamacrocyclic complexes with a threadlike structure, which could be promising docking units in surface-immobilized rotaxanes.

[a] U. E. Wawrzyniak, S. Domagała, E. Maicka, Prof. R. Bilewicz, Prof. K. Woźniak
Department of Chemistry, University of Warsaw
Pasteura 1, 02-093 Warszawa (Poland)
Fax: (+48) 22-822-0211 ext 345
E-mail: bilewicz@chem.uw.edu.pl
kwozniak@chem.uw.edu.pl

[b] M. Woźny, J. Kowalski, Dr. B. Korybut-Daszkiewicz
Institute of Organic Chemistry, Polish Academy of Sciences
Kasprzaka 44/52, 01-224 Warszawa (Poland)
Fax: (+48) 22-632-6681
E-mail: bkd@icho.edu.pl

We characterize the kinetics of electron transfer through these two types of complexes immobilized on gold surfaces and show their interactions with acceptors that are present in the solution.

Results and Discussion

Synthesis: The synthesis of the dithiol derivatives of nickel(II) and copper(II) complexes **5·Ni** and **5·Cu** is summarized in Scheme 1. Transesterification of previously described dimethyl esters **1·Ni** and **1·Cu**[12] with 1,3-propylene glycol in the presence of sodium gave diols **2·Ni** and **2·Cu**. Treating **2·Ni** and **2·Cu** with mesyl chloride in the presence of triethylamine resulted in the formation of dimesyl esters **3·Ni** and **3·Cu**, which were subsequently transformed into dithiols **5·Ni** and **5·Cu** after treatment with thiourea. The structures of the studied complexes were confirmed by elemental analyses, ESI or FD mass spectroscopy, and in the case of diamagnetic nickel(II) complexes, by ^{1}H and ^{13}C NMR spectroscopy.

Structure: Compound **5·Ni** formed crystals of suitable quality to allow single-crystal X-ray investigations. It crystallizes in the triclinic $P\bar{1}$ space group with one molecule in the asymmetric unit cell (see Figure 1), which results in two molecules per unit cell related by an inversion center.

The 14-membered tetraazamacrocyclic ring of the molecule contains a Ni^{II} ion and is functionalized with two 3-mercaptopropoxycarbonyl groups at the *meso* positions. The macrocyclic part of the molecule is almost planar, with the exception of ethylene linkers, and is coplanar with the ester part of the 3-mercaptopropoxy chain. The torsion angle values are 3.4(3) and −3.2(3)° for the C9-C10-C11-O1 and C6-C5-C15-O4 molecular fragments, respectively. The planarity of the macrocyclic ring was estimated by fitting the least-square best-plane (denoted hereafter as L^1) to selected atoms of the macrocyclic ring. All atoms, except the ethylene bridges, constituting the ring were selected for definition of the L^1 plane. The root mean square (rms) deviation of the fitted atoms from the plane L^1 is 0.08 Å. The second plane L^2 was defined as the atoms of the ethylene linkers and the value of the angle between the L^1 and L^2 planes is 26.1(1)°. Both parameters are in good agreement with our previous reports on 14-membered tetraazamacrocyclic Ni and Cu complexes.[8,9,12] The average value of the Ni–N bonds is 1.854(1) Å, and the other parameters, such as bond lengths and angles, which characterize the macrocyclic ring, are in accordance with previously reported Ni complexes.[8,9,12] Important bonds and angles are presented in Table 1.

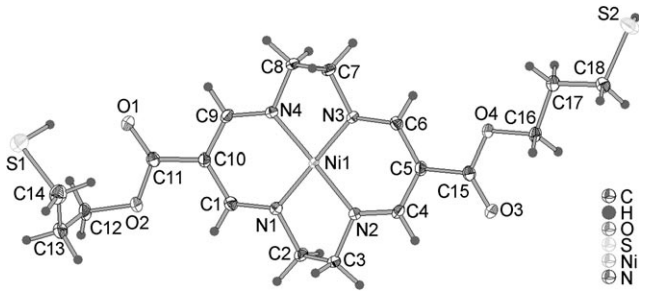

Figure 1. Thermal ellipsoids (at the 50% probability level) and atom numbering scheme of the **5·Ni** molecule.

Two 3-mercaptopropoxy chains are located *trans* to each other, with the -$(CH_2)_3$–SH ends in both *gauche* and *anti* conformations. The absolute values of the torsion angles (calculated using the non-hydrogen atoms) are 67 and 175°, respectively. These conformations allow the -SH groups to form intra- and intermolecular hydrogen bonds to the oxygen atom of the carbonyl group (see Table 2 and Figure 2).

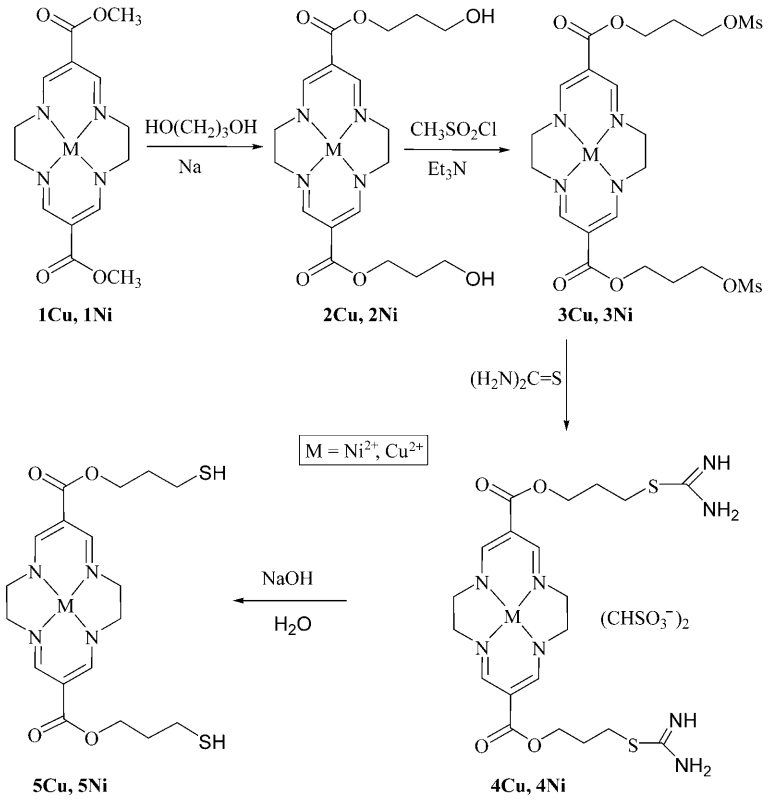

Scheme 1. Synthesis of complexes **5·Ni** and **5·Cu**.

Table 1. Selected bond lengths and nonbonding distances for **5·Ni**.

Parameter	Distance [Å]	Parameter	Distance [Å]
L[1]···Ni[a]	3.446(2)	N2–C3	1.469(3)
Ni1···Ni1[a]	6.6010(7)	N3–C6	1.314(3)
Ni1···Ni[b]	7.8883(7)	N3–C7	1.479(3)
S2···S2[c]	3.487(2)	N4–C9	1.309(3)
Ni1–N1	1.854(2)	N4–C8	1.477(3)
Ni1–N2	1.854(2)	C1–C10	1.408(3)
Ni1–N3	1.849(2)	C2–C3	1.516(3)
Ni1–N4	1.859(2)	C4–C5	1.404(3)
S1–C14	1.808(2)	C5–C6	1.413(3)
S2–C18	1.803(2)	C5–C15	1.461(3)
O1–C11	1.221(3)	C7–C8	1.521(3)
O2–C11	1.353(3)	C9–C10	1.411(3)
O2–C12	1.450(2)	C10–C11	1.461(3)
O3–C15	1.215(3)	C12–C13	1.511(3)
O4–C15	1.357(3)	C13–C14	1.522(3)
O4–C16	1.450(2)	C16–C17	1.514(3)
N1–C1	1.308(3)	C17–C18	1.521(3)
N1–C2	1.470(3)	N2–C4	1.313(3)

Symmetry transformations: [a] $1-x$, $1-y$, $1-z$; [b] $2-x$, $1-y$, $1-z$; [c] $1-x$, $-y$, $2-z$.

Table 2. Geometry of the hydrogen bonds in complex **5**–**Ni**.[a]

DH···A	Symmetry	d(DH) [Å]	d(H···A) [Å]	d(D···A) [Å]	$\measuredangle$(DHA) [°]
S1H1S···O1	x, y, z	1.23(3)	2.34(3)	3.463(2)	151(2)
S2H2S···O1	$2-x, 1-y, 1-z$	1.15(3)	2.42(3)	3.481(2)	153(2)

[a] D = donor, A = acceptor.

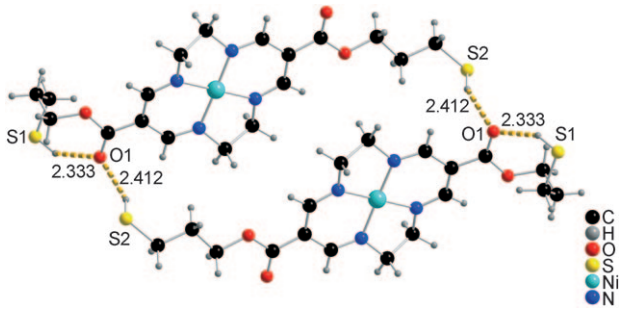

Figure 2. Bismacrocyclic unit formed by hydrogen bonds between the **5·Ni** molecules.

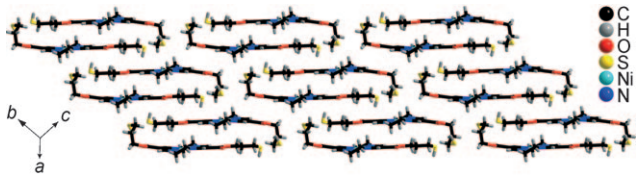

Figure 3. Crystal packing of the **5·Ni** molecules.

The crystal packing of the molecules is shown in Figure 3. The molecules create moderately shifted stacks of dimeric-like substructures in the crystal lattice. The molecules that form dimers are shifted towards the 3-mercaptopropoxy functional groups of the neighbouring molecules. The relative distance between two molecules in a dimer, measured between the metal centers, is 6.6010(7) Å (3.446(2) Å between the planes of the macrocyclic rings), whereas the closest distance (Ni–Ni) between two dimeric structures is 7.8883(7) Å. The packing slightly resembles that of the bis-macrocyclic structures.[12] The molecules in dimers are interacting mainly through π–π and weak interactions of C–H···X type. Note that the sulfur atoms create not only hydrogen bonds, but also weak S–S-type interactions between the dimers, with a S–S distance of 3.487(1) Å.

Electrochemistry: Cyclic voltammograms obtained for the gold electrode modified with macrocyclic complexes of nickel(II) and copper(II) are shown in Figure 4. All of the peaks

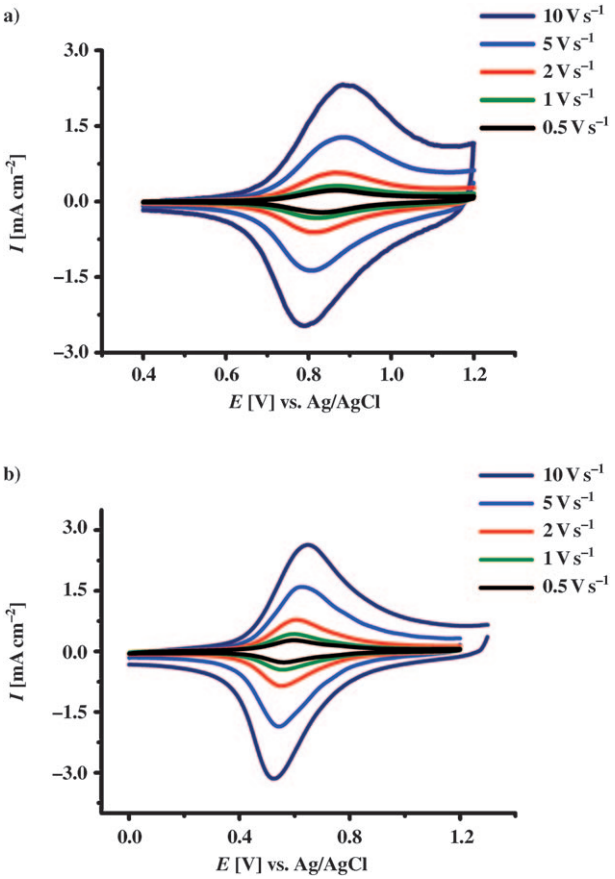

Figure 4. Cyclic voltammograms recorded by using a gold electrode modified by a) **5·Ni** and b) **5·Cu** in 0.1 M TBAHFP/acetonitrile; scan rates: 0.5, 1, 2, 5, and 10 V s^{-1}.

are reproducible in multicyclic voltammetric runs except the first, which is usually larger due to an excess of poorly adsorbed molecules. The oxidation of the Ni^{II} complex takes place at a potential that is 210 mV more positive than that of the Cu^{II} center. The electrode is not totally covered by the complexes because of their bulky 3D structure, so the peak of **5·Ni** oxidation appears close to the onset of gold oxidation, which may lead to a partial destruction of the monolayer under longer cycling. For both of the macrocyclic complexes immobilized on the electrode surface, the peaks are broader compared with the theoretical prediction

(90.6 mV for a one-electron process at room temperature). In the case of **5·Ni**, the widths at half-height are 148 and 170 mV for the anodic and cathodic peaks, respectively (scan rate 0.5-1 $V s^{-1}$). The peak broadening may be attributed to different orientations of the molecules or to intermolecular interactions between the metal centers in the monolayer. The peak separation is constant for the scan rates lower than 1 $V s^{-1}$. Although the heights of the peaks for both macrocyclic complexes are similar, the half-widths of the **5·Cu** peaks (112 and 156 mV for the anodic and cathodic peak, respectively), and the peak-to-peak separations are slightly smaller.

These macrocyclic complexes can be attached to the surface by one or two thiol groups, as shown schematically in Figure 5. The surface concentration of **5·Ni** molecules, evaluated from the charge of the oxidation peak by using the equation $\Gamma = Q/nFA$, is approximately $(2.58 \pm 0.35) \times 10^{-10}$ mol cm^{-2}. Hence, the area per molecule in this monolayer is (64.4 ± 5.9) Å^2, which indicates that the molecules are oriented perpendicular to the electrode surface (Figure 5); this would be advantageous when the molecule is used as a rotaxane axis. The mean surface coverage of **5·Cu** is approximately $(3.43 \pm 0.29) \times 10^{-10}$ mol cm^{-2} and the area per molecule is (48.4 ± 4.4) Å^2. The **5·Cu** complex monolayer is packed more densely than that of **5·Ni**.

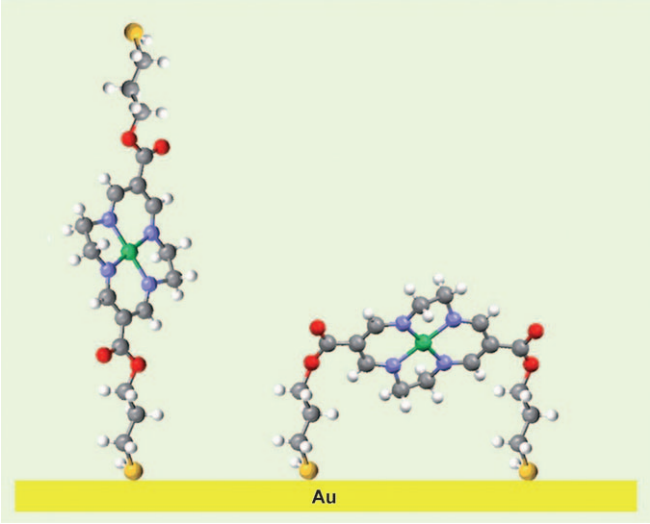

Figure 5. Schematic representation of the two binding modes of tetraazamacrocyclic complexes to the gold electrode surface.

When self-assembly of **5·Cu** was carried out in a 1 mM solution at room temperature for a longer time (48–96 h), we obtained a split voltammetric curve (first scan) with two oxidation peaks (Figure 6). After further voltammetric cycles, the peaks merged into single cathodic and anodic peaks. The widths at half-height, for both the oxidation and reduction peaks, are smaller than expected for the ideal one-electron process. This reflects some attractive interactions between the oxidized form of Cu and the anions in the solution (PF_6^- anions are present in the supporting electrolyte).

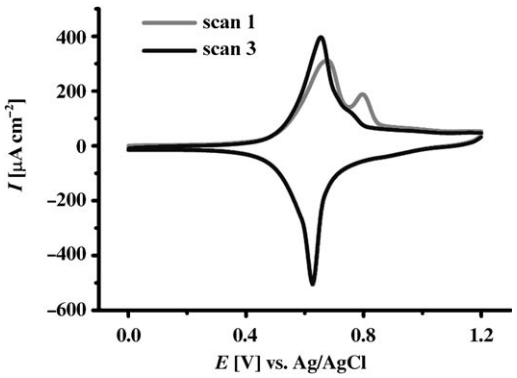

Figure 6. Cyclic voltammograms recorded for a gold electrode modified with **5·Cu**; scan rate = 0.5 $V s^{-1}$.

At these very long self-assembly times, the background current is also smaller than at shorter self-assembly times. Larger charges of the peaks and smaller background currents may indicate oxidation of some terminal SH groups and formation of more than one monolayer at the electrode surface. The peak splitting usually indicates different molecular orientations in the surface layer (Figure 6).

Two differently oriented populations of molecules can be formed during spontaneous organization of **5·Cu** on the electrode surface. However, cycling the potential has an organizing effect and produces a well-packed monolayer of molecules oriented perpendicularly to the electrode surface. Interestingly, this effect was not seen in the case of the **5·Ni** monolayer on the gold electrode.

The peak currents of **5·Ni** and **5·Cu** immobilized on gold increase linearly with scan rate as predicted for the surface-adsorbed species (Figure 7a and c). At values higher than 25 $V s^{-1}$, not all of the centers undergo the electrode processes, and deviations from linearity are observed (Figure 7b and d). This confirms that the orientation of all molecules is not identical, and at low scan rates, some of the molecules can be oxidized through lateral charge transport within the monolayer.

The electrode kinetics become visible at higher scan rates (Figure 8). The oxidation and reduction peak potentials shift to more positive and more negative values, respectively. At scan rates above 67 (nickel center) and 55 $V s^{-1}$(copper center), the peak separation begins to increase, indicating the limitation arising from the charge-transfer kinetics. The values of the peak separation, ΔE, were proportional to the logarithm of the scan rate as predicted by the Laviron theory.[14,15] The plots of the anodic and cathodic peak potential as a function of scan rate are shown in Figure 8.

The standard rate constants of the electrode process for the Ni^{II} macrocyclic complex immobilized on the electrode surface were calculated from such voltammograms by using the Laviron treatment.[14,15] The value of k_s is obtained from the equation, $k = \alpha n F v_c / RT = (1\text{-}\alpha) n F v_a / RT$, and is $(1.7 \pm 0.07) \times 10^2$ s^{-1}. The scan rate corresponding to the intersection point of the two asymptotes, $v_a = v_c$ is obtained from Figure 5a. The electron-transfer rate constant through the monolayer formed by the Cu^{II} macrocyclic complex was cal-

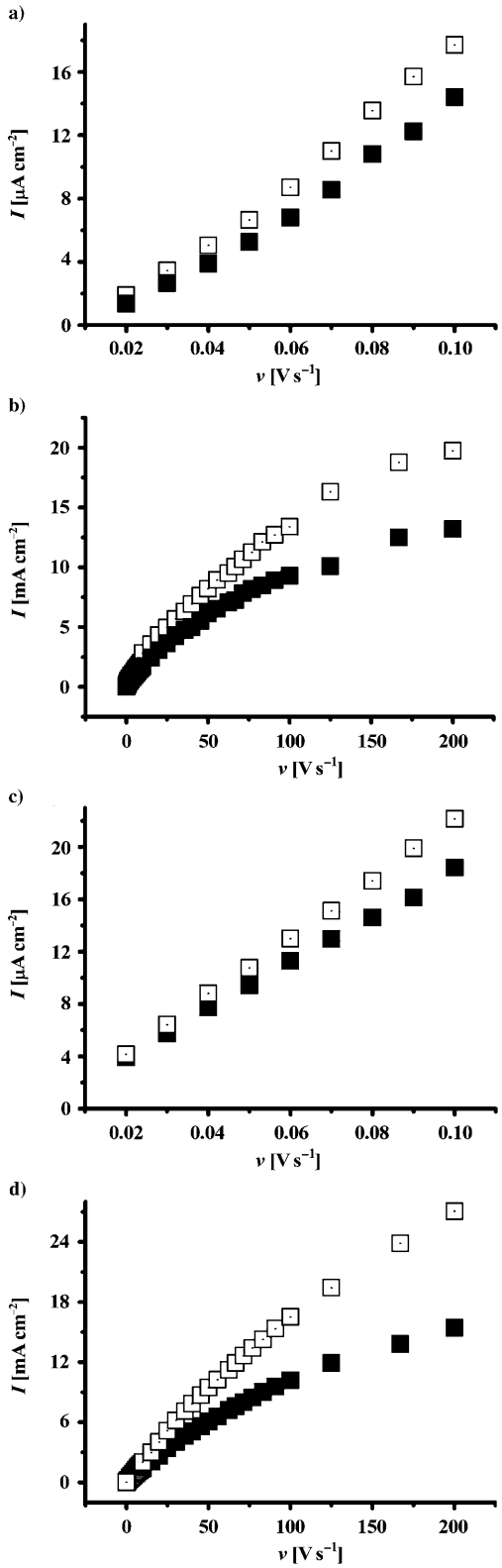

Figure 7. Voltammetric peak current versus scan rate dependence for a gold electrode modified by: a),b) **5·Ni** and c),d) **5·Cu**. Supporting electrolyte 0.1 M TBAHFP/acetonitrile.

culated by using the same equation, and is $(1.86\pm0.04)\times 10^2\ s^{-1}$, in which $v_a = v_c = 24.3\ V\,s^{-1}$.

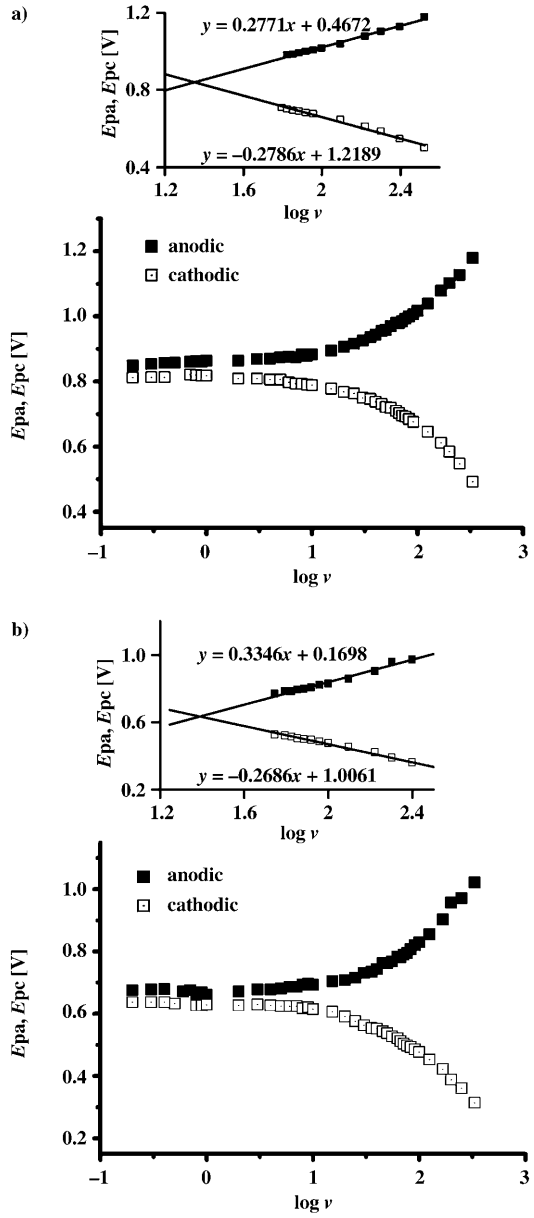

Figure 8. Voltammetric peak potential versus scan rate dependencies for a gold electrode covered with a) **5·Ni** monolayer and b) **5·Cu** monolayer. Supporting electrolyte 0.1 M TBAHFP/acetonitrile.

The transfer coefficient (α) was obtained by measuring the variation of the peak potential with the scan rate. A plot of E_p versus $\log v$ yields two straight lines with slopes equal to $2.3RT/\alpha nF$ and $2.3RT/(1\text{-}\alpha)nF$ for the anodic and cathodic peaks, respectively, to give values of $\alpha_a = 0.79$, $\alpha_c = 0.21$ for **5·Ni,** and $\alpha_a = 0.82$, $\alpha_c = 0.22$ for **5·Cu**.

To get a more ordered and upright oriented molecular layer, the electrode surface was covered by a mixed monolayer of **5·Cu** and hexanethiol (1:4 molar ratio in the self-assembly solution). The STM images of electrodes covered by a mixed- and single-component hexanethiol monolayer are shown in Figure 9. The lighter spots indicate the anchored dithiolated complex **5·Cu** protruding above the hexanethiol

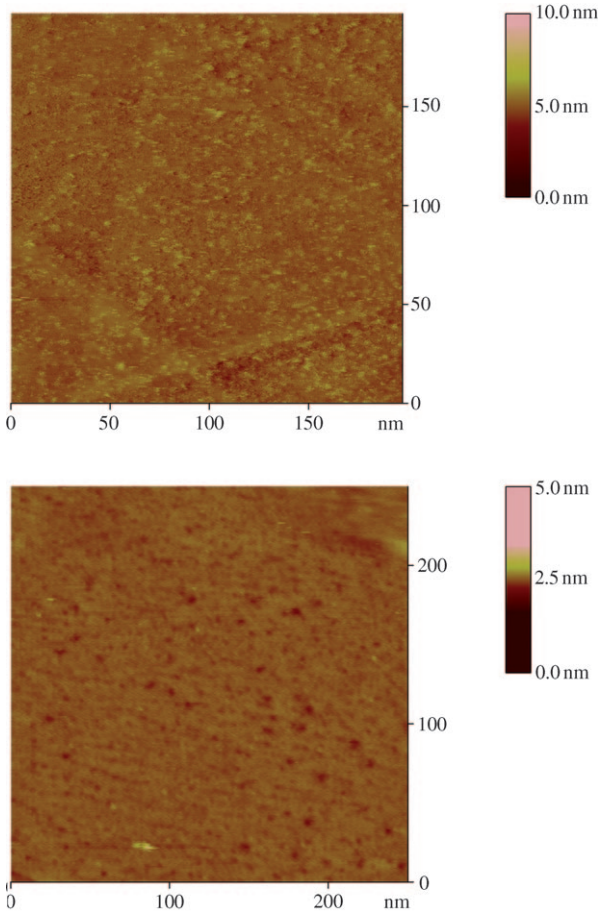

Figure 9. STM images of a) **5·Cu** and hexanethiol (1:4) molar ratio and b) monolayer of pure hexanethiol. Imaging conditions: bias voltage V = 1000 mV; tunneling current I = 70 pA.

matrix (Figure 9a). The height of the spikes observed in the 3D STM image is in the range 1.8–2.5 nm, which corresponds to the size of the **5·Ni** analogue molecules (2.8 nm), based on the crystallographic data (see Table 1). The upright position of the active sites of the dithiol complex was checked by covering the surface with a gold colloid. The numerous Au droplets bound to the protruding thiol groups are easily detected on the STM image.

The peak characteristics for monocomponent and mixed monolayers are shown in Table 3 and the current versus

Table 3. Characteristics of a single component and a mixed monolayer.[a]

Layer			**5·Cu**	
	Ep [V]	ip [μA]	$b_{1/2}$ [mV]	K [$\times 10^2$ s^{-1}]
Oxidation peak	0.623 ± 0.012	6.67 ± 1.11	120 ± 0.08	1.92 ± 0.09
Reduction peak	0.589 ± 0.010	7.26 ± 1.20	154 ± 0.02	1.84 ± 0.14
Layer			**5·Cu** + hexanethiol	
	Ep [V]	ip [μA]	$b_{1/2}$ [mV]	K [$\times 10^2$ s^{-1}]
Oxidation peak	0.632 ± 0.004	3.4 ± 1.2	186 ± 0.002	2.48 ± 0.39
Reduction peak	0.595 ± 0.004	3.17 ± 0.9	145 ± 0.004	2.42 ± 0.31

[a] Voltammograms recorded at 1 V s^{-1}. Ep = peak potential; ip = peak current; $b_{1/2}$ = peak width at half height.

scan rate dependencies are shown in Figure 10. The mixed monolayers show very good stability, and in practice no changes are observed upon numerous voltammetric scans. The rate constants are slightly increased compared with

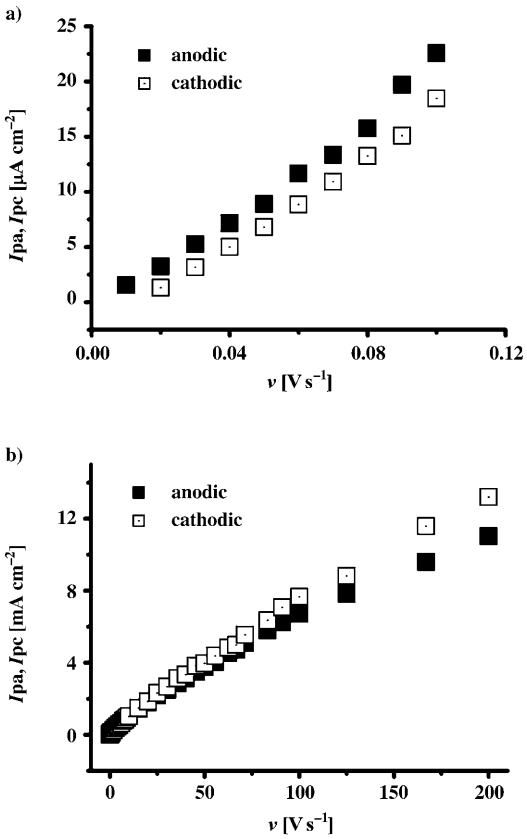

Figure 10. Voltammetric peak current versus scan rate dependence for a gold electrode modified by **5·Cu** + hexanethiol. Supporting electrolyte: 0.1 M TBAHFP/acetonitrile. a) Low and b) high scan rate ranges.

those obtained for a single-component layer. The k values obtained from the cyclic voltammograms have to be treated as approximate values, because at the highest scan rates the current resistance (IR) drop should also be taken into account.[16–23] The value of the rate constant obtained for the **5·Cu** + hexanethiol monolayer, measured by using chronoamperometry, is somewhat higher, at (7.72 ± 0.10) × 10^2 s^{-1}.

The mixed monolayer is more uniformly organized in terms of orientation of the molecules, because the diluent hexanethiol only has one terminal SH group. Thus, one favored, perpendicular orientation is achieved. In addition, the longer **5·Cu** molecules extend above the diluent hexanethiol, and are susceptible to interactions with solution species. This should be a good strategy for building rotaxanes directly on electrodes. We used a charged Ni,Ni-bismacrocyclic complex (**7·NiNi**; see Figure 11)[8] to detect interactions between the anchored monolayer and acceptor molecules in the solution. In this case, a water/acetonitrile (3:7 v/v) mixture was used as the solvent to enhance the affinity of the

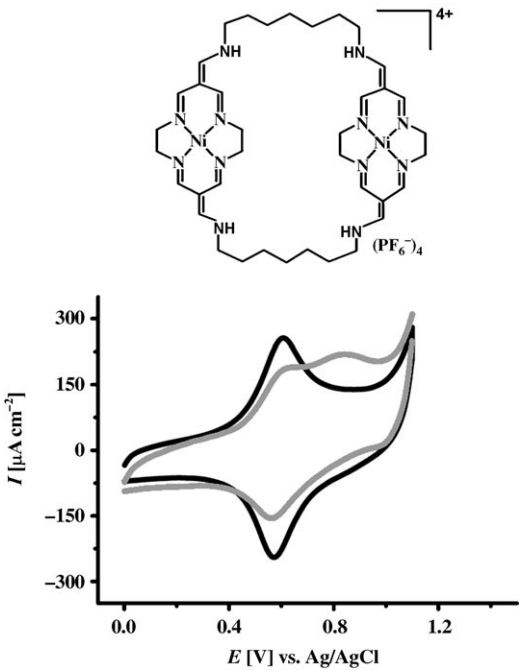

Figure 11. Cyclic voltammograms recorded by using a gold electrode modified by **5·Cu**+hexanethiol mixed monolayer in 0.1 M TBAHFP/acetonitrile, containing 0 (black line) and 1.75×10^{-4} M **7·NiNi** (gray line); scan rate: 0.5 V s^{-1}.

bismacrocycle towards the modified electrode. Without water the results were not reproducible, although peak splitting was often observed. The **7·NiNi** complex affected the donor abilities of the **5·Cu** molecules, which were self-assembled on the gold surface. The presence of the second peak at a more positive potential reflects the interactions with solution species, leading to a decrease in the donor abilities of the self-assembled **5·Cu** complex. Two types of interactions should be considered: the first one is the pseudorotaxane-type threading of the bismacrocycle onto the anchored **5·Cu** moieties, and the second is the binding of the dangling thiol group to the Ni center of the bismacrocyclic complex. However, large peak splitting indicates the first type of interaction because additional binding through the terminal SH group should not change the potential of the distant Cu center by much. The coordination, which is close to square-planar, is common for these types of Ni^{II} complexes. The oxidation to Ni^{III} appears at a much more positive potential (1.326 V) than that applied in the present study, as shown in our recent paper.[24] In the oxidized form the **5·Cu** complex becomes positively charged and repulsion of the solution species takes place; this also suggests a pseudorotaxane type of interaction. The formation of such host–guest complexes with **5·Cu** in the gas phase was revealed by analyzing the ESI mass spectra (ESIMS).[12] Herein, we demonstrate that immobilization of the donor unit on the electrode does not remove such interactions; on the contrary it may enhance them and lead to the formation of a pseudorotaxane structure. These observations also indicate the possibility of tuning the donor–acceptor properties of the molecules by interacting them with appropriate ligands in the solution.

Conclusion

New derivatives of neutral macrocyclic complexes functionalized with 3-mercaptopropyl groups were synthesized and the crystal structure of **5·Ni** was established. These dithiolated transition-metal complexes self-assemble into well-organized, single-component, and mixed monolayers on gold electrodes. Hexanethiol as the "diluent" in the mixed monolayer provides more uniform packing, with the macrocyclic units emerging above the alkanethiol matrix. These active donor sites interact with the cyclic acceptor cations in the solution, leading to the formation of pseudorotaxane structures on the electrode surface. The interactions between the pseudorotaxane components are switched off upon application of the appropriate potential at which the surface-immobilized complex is oxidized.

Experimental Section

General: The NMR spectra were obtained on Varian Mercury 400 and Varian Gemini 2000BB spectrometers. Signals are reported in ppm relative to the residual solvent signal. IR spectra (paraffin oil mulls) were recorded with a Perkin–Elmer Spectrum 2000 FTIR spectrometer. ESIMS and FDMS were measured on Mariner Perseptive Biosystem and Walters Micromass GCT Premier mass spectrometers, respectively.

Synthesis: {6,13-bis(metoxycarbonyl)-1,4,8,11-tetraazacycloteradca-4,6,11,13-tetraenato(2-)-$\kappa^4N^{1,4,8,11}$}nickel(II) and copper(II) complexes (**1·Ni** and **1·Cu**) were obtained according to procedures described elsewhere.[12]

Complex 2·Ni: Sodium (0.17 g, 7.40 mmol) was dissolved in 1,3-propanediol (80 mL) before complex **1·Ni** (1 g, 2.74 mmol) was added, and the mixture was stirred for 4 h at 100 °C. The resulting dark-orange solution was poured into distilled water (200 mL) and left overnight in the refrigerator. The orange precipitate was filtered off and washed with a small amount of methanol. The crude product was dissolved in a dichloromethane/methanol mixture, and crystallized upon slow evaporation of the solvents. The orange crystals were dried in vacuo over P_2O_5 (0.90 g, 72.4 %). M.p. 188–190 °C; ^{1}H NMR (400 MHz, $CDCl_3$, TMS): $\delta=1.88$ (q, $^3J=6.0$ Hz, 4H; CH_2 β to -OH), 2.52 (t, $^3J=6.1$ Hz, 2H; -OH), 3.39 (br, s, 8H; N–CH_2-), 3.66 (q, $^3J=6.0$ Hz, 4H; CH_2 α to -OH), 4.35 (t, $^3J=5.9$ Hz, 4H; CH_2 γ to -OH), 7.82 ppm (s, 4H; -CH=N); ^{13}C NMR (100 MHz, $CDCl_3$, TMS): $\delta=32.5$ (-CH_2- β to -OH), 58.8 (-CH_2- γ to -OH), 59.8 (-CH_2- α to -OH), 58.6 (N-CH_2-), 97.9 (ring -C=), 155.0 (-CH=N), 168.6 ppm (C=O); ESIMS: *m/z* (%): 452.1 [$C_{18}H_{26}N_4O_6Ni$]$^+$; elemental analysis calcd (%) for $C_{18}H_{26}N_4O_6Ni$ ($M=453.12$ g mol^{-1}): C 47.7, H 5.8, N 12.4; found: C 47.5, H 5.7, N 12.

Complex 2·Cu: Complex **2·Cu** was obtained from **1·Cu** following the same procedure as above. Yield: 56.3 %; IR (Nujol): $\bar{\nu}=3416$ (m, br), 1658 (m), 1599 (s,) 1547 (m), 1267 (s), 1133 cm^{-1}(m); ESIMS: *m/z* (%): 457.1 [$C_{18}H_{26}N_4O_6Cu$]$^+$; elemental analysis calcd (%) for $C_{18}H_{26}N_4O_6Cu$ (457.97): C 47.2, H 5.7, N 12.2; found: C 46.8, H 5.9, N 12.1.

Complex 3·Ni : Complex **2·Ni** (0.33 g, 0.73 mmol) and triethylamine (0.42 mL, 3.02 mmol) were added to stirred dichloromethane (30 mL). Methanesulfonyl chloride (0.215 mL, 2.78 mmol) was carefully added, and the mixture was heated at reflux for 6 h. After cooling, the mixture was diluted with ethanol (50 mL), and the product was precipitated upon slow evaporation of the solvents (0.35 g, 79.5 %). ^{1}H NMR (400 MHz, $CDCl_3$, TMS): $\delta=2.13$ (q, $^3J=6.1$ Hz, 4H; CH_2 β to -OMs), 3.03 (s, 6H;

S-CH_3), 3.40 (br, s, 8H; N-CH_2), 4.29 (t, $^3J=6.0$ Hz, 4H; CH_2 α to -OMs), 4.35 (t, $^3J=6.2$ Hz, 4H; CH_2 γ to -OMs), 7.81 ppm (s, 4H; -CH=N); ^{13}C NMR (100 MHz, $CDCl_3$, TMS): $\delta=28.9$ (CH_2 β -OMs), 59.0 (CH_2 γ to -OMs), 66.8 (CH_2 α to -OMs), 37.4 (S–CH_3), 58.8 (N-CH_2), 97.9 (ring -C=), 154.9 (-CH=N), 167.5 ppm (C=O); IR (Nujol): 1662 (m), 1595 (s), 1540 (s), 1275 (s), 1172 (s), 1122 cm^{-1} (s); ESIMS: *m/z* (%): 608.0 $[C_{20}H_{30}N_4O_{10}S_2Ni]^+$, 631.0 $[C_{20}H_{30}N_4O_{10}S_2Ni+Na]^+$; elemental analysis calcd (%) for $C_{20}H_{30}N_4O_{10}S_2Ni$ ($M=609.30$): C 39.4, H 5.0, N 9.2; found: C 39.6, H 4.9, N 9.2.

Complex 3·Cu: Complex **3·Cu** was obtained from **2·Cu** following the same procedure as above. Yield: 91.0%; IR (Nujol): 1664 (m), 1598 (s), 1550 (m), 1265 (s), 1171 cm^{-1} (m); ESIMS: *m/z* (%): 614.0 $[C_{20}H_{30}N_4O_{10}S_2Cu+H^+]^+$, 636.0 $[C_{20}H_{30}N_4O_{10}S_2Cu+Na^+]^+$; elemental analysis (%) calcd for $C_{20}H_{30}N_4O_{10}S_2Cu$ ($M=614.16$): C 39.1, H 4.9, N 9.1; found: C 38.6, H 5.0, N 9.0.

Complex 4·Ni: Complex **3·Ni** (0.347 g, 0.57 mmol) and thiourea (0.445 g, 5.85 mmol) were dissolved in dimethylformamide (7 mL) and the resulting mixture was stirred at 55°C for 6 h. The solution was then diluted with 2-propanol (70 mL) and left for 12 h in the refrigerator. The orange solid was filtered off, washed with a small amount of 2-propanol, and dried in vacuo (0.376 g, 86.6%). ^{1}H NMR (200 MHz, D_2O, TMS): $\delta=$ 2.00 (q, $^3J=6.2$ Hz, 4H; CH_2 β to -S(NH_2)C=NH_2^+), 2.71 (s, 6H; S–CH_3), 3.12 (t, $^3J=6.7$ Hz, 4H; CH_2 α to -S(NH_2)C=NH_2^+), 3.30 (br, s, 8H; N–CH_2), 4.09 (t, $^3J=5.5$ Hz, 4H; CH_2 γ to -S(NH_2)C=NH_2^+), 7.74 ppm (s, 4H; -CH=N), signals of -S(NH_2)C=NH_2^+ invisible due to fast exchange with solvent; IR (Nujol): 1665 (m), 1648 (m), 1590 (s), 1556 (m), 1279 cm^{-1} (s); ESIMS: *m/z* (%): 285.1 $[C_{20}H_{32}N_8O_4S_2Ni]^{2+}$, 571.1 [$C_{20}H_{32}N_8O_4S_2Ni$-$H^+]^+$; elemental analysis calcd (%) for $C_{20}H_{32}N_8O_4S_2Ni{\cdot}2CH_3SO_3$ ($M=761.52$): C 34.7, H 5.0, N 14.7; found: C 34.9, H 5.2, N 14.5.

Complex 4·Cu: Complex **4·Cu** was obtained from **3·Cu** following the same procedure as above. Yield 62.0%; IR (Nujol): 1662 (m), 1649 (m), 1587 (s), 1553 (m), 1278 (s), 1130 cm^{-1} (m); ESIMS: *m/z* (%): 287.9 $[C_{20}H_{32}N_8O_4S_2Cu]^{2+}$, 574.5 $[C_{20}H_{32}N_8O_4S_2Cu$-$H^+]^+$; elemental analysis calcd (%) for $C_{20}H_{32}N_8O_4S_2Cu{\cdot}2CH_3SO_3$ ($M=766.37$): C 34.5, H 5.0, N 14.6; found: C 34.6, H 5.2, N 14.4.

Complex 5·Ni: Complex **4·Ni** (0.396 g, 0.52 mmol) was added to deoxygenated water (10 mL). The mixture was stirred under argon at 60°C until it became homogeneous. After cooling to 5°C, NaOH (2 g) was added whilst stirring vigorously, and ensuring the temperature was below 20°C. After 3 h, the cooled suspension was acidified with concd hydrochloric acid (8 mL). The mixture was then stirred for a further hour, and the precipitate was filtered off, washed well with deoxygenated water, and immediately dried in vacuo over P_2O_5 (0.232 g, 97.8%). ^{1}H NMR (400 MHz, $CDCl_3$, TMS): $\delta=1.43$ (t, $^3J=8.1$ Hz, 2H; -SH), 1.97 (q, $^3J=$ 6.0 Hz, 4H; CH_2 β to -SH), 2.61 (q, $^3J=7.5$ Hz, 4H; CH_2 α to -SH), 3.38 (br, s, 8H; N–CH_2), 4.25 (t, $^3J=6.1$ Hz, 4H; CH_2 γ to -SH), 7.89 ppm (s, 4H; -CH=N); ^{13}C NMR (100 MHz, $CDCl_3$, TMS): $\delta=21.4$ (CH_2 α to -SH), 33.4 (CH_2 βto -SH), 61.4 (CH_2 γ to -SH), 58.8 (N–CH_2), 98.2 (ring -C=), 154.9 (-CH=N), 167.7 ppm (C=O); IR (Nujol): 1669 (s), 1598 (s), 1537 (m), 1272 (m), 1117 cm^{-1} (m); FDMS: *m/z* (%): 484.1 $[C_{18}H_{26}N_4O_4S_2Ni]^+$; elemental analysis calcd (%) for $C_{18}H_{26}N_4O_4S_2Ni$ ($M=485.24$): C 44.6, H 5.4, N 11.5; found: C 44.6, H 5.2, N 11.7.

Complex 5·Cu: Complex **5·Cu** was obtained from **4·Cu** following the same procedure as above. Yield 57.2%; IR (Nujol): 1674 (m), 1599 (s), 1538 (m), 1260 (s), 1117 cm^{-1} (m); FDMS: *m/z* (%): 489.4 $[C_{18}H_{26}N_4O_4S_2Cu]^+$; elemental analysis calcd (%) for $C_{18}H_{26}N_4O_4S_2Cu$ ($M=490.09$): C 44.1, H 5.3, N 11.4; found: C 43.8, H 5.5, N 11.6.

Voltammetry: Cyclic voltammetry was performed by using a CHI 750B potentiostat (CH Instrument, Austin, USA) in the three electrode arrangement, with silver/silver chloride (Ag/AgCl) as the reference, platinum foil as the counter electrodes, and the monolayer-modified gold electrodes (Arrandee) as the working electrode. Acetonitrile containing 0.1 M tetrabutylammonium hexafluorphosphate (TBAHFP) was used as the supporting electrolyte solution. The reference electrode was separated from the working solution by an electrolytic bridge filled with 1 M TBAHFP/acetonitrile solution. The reference electrode potential was calibrated by using a ferrocene electrode process in the same TBAHFP/acetonitrile solution. Argon was used to deaerate the solution and an argon blanket was maintained over the solution during the experiments. All electrochemical experiments were carried out at 25°C.

Electrode preparation: The gold electrodes were sequentially mechanically polished with 1.0, 0.3 and 0.05 μm alumina powder, and rinsed thoroughly with acetonitrile. They were then electrochemically cleaned by potential cycling in a 0.5 M solution of H_2SO_4 in the potential range 0–1.4 V at a scan rate of 0.1 $V s^{-1}$ until stable voltammograms, typical of clean gold were obtained. After this procedure, the substrates were transferred to the coating solution. Self-assembly was carried out from a 1 mM solution of **5·Ni** or **5·Cu** in a mixture of ethanol and chloroform (1:1) for 24 h at room temperature, and then the modified substrates were washed with ethanol and acetonitrile and immersed into the supporting electrolyte solution. The mixed **5·Cu**–hexanethiol monolayer was prepared by using deaerated solutions of 1 mM **5·Cu** and 1 mM hexanethiol in chloroform/ethanol (1:1; or otherwise stated). During the self-assembly process, the solution was kept under an inert atmosphere to prevent oxidation of the SH groups and the formation of multilayers.[10–12] In the STM experiments a Nanoscope III (Digital Instruments, Santa Barbara, CA) microscope and commercially available Pt–Ir tips were used. Gold 200 nm thick was evaporated on glass with a pre-layer of 2–4 nm of chromium (Gold Arrandee, Gmbh), were used as the working electrodes. The monolayers of Ni or Cu macrocycles were self-assembled on gold substrates. Before monolayer deposition the substrates were flame annealed until the sample glowed dark red, and then cooled to room temperature.[14]

X-ray investigations: Single-crystal X-ray measurements of **5·Ni** were performed on a BRUKER APEX II ULTRA κ-axis diffractometer with a TXS rotating anode using $Mo_{K\alpha}$ radiation at 90 K. The crystal was positioned at 60 mm from the APEXII 4 K CCD detector. Data collection was done by using a combination of 5 ϕ and ω runs, with 0.5 degrees scan width, to give a total of 2196 frames and a counting time of 15 s. The data were corrected for Lorentz and polarization effects. No absorption correction was applied. Indexing, integration, and scaling were performed with original Bruker Apex II software.[25]

The structure was solved by direct methods[26] and refined by using SHELXL.[27] The refinement was based on F^2 for all reflections except those with very negative F^2. Weighted *R* factors *wR* and all goodness-of-fit *S* values are based on F^2. Conventional *R* factors are based on *F* with *F* set to zero for negative F^2. The $F_0^2 > 2\sigma(F_0^2)$ criterion was used only for calculating *R* factors, and is not relevant to the choice of reflections for the refinement. The *R* factors based on F^2 are about twice as large as those based on *F*. All hydrogen atoms were located in idealized averaged geometrical positions and allowed to ride at the heavy atoms, except the thiol H atoms, which were located from a differential map and refined isotropically. Scattering factors were taken from Tables 6.1.1.4 and 4.2.4.2 in reference[28].

5·Ni: $C_{18}H_{26}N_4NiO_4S_2$; $M_W=485.26$; $T=90$ K; $\lambda=0.71073$ Å; triclinic; space group $P\bar{1}$; unit cell dimensions: $a=9.1449(9)$, $b=10.0849(9)$, $c=$ 12.049(1) Å; $\alpha=94.283(2)$, $\beta=90.372(2)$, $\gamma=113.433(1)°$; $V=$ 1015.9(2) $Å^3$; $Z=2$; $\rho_{calcd}=1.586$ $mg m^{-3}$; absorption coefficient: 1.194 mm^{-1}; $F(000)=508$; crystal size: $0.15\times0.08\times0.05$ mm; θ range for data collection: 2.43–25.00°; index ranges: $-10 \le h \le 10$, $-11 \le k \le 11$, $-14 \le l \le 4$; reflections collected: 12304; independent reflections: 3561 [$R_{int}=0.0309$]; refinement method: full-matrix least-squares on F^2; data/restraints/parameters: 3561/0/270; goodness-of-fit on $F^2=1.048$; final *R* indices [$I > 2\sigma(I)$]: $R1=0.0288$ and $wR2=0.0746$; *R* indices (all data): $R1=0.0327$ and $wR2=0.0773$; weight $=1/[\sigma^2(F_o^2) + (0.0372P)^2 + 0.8602P]$ in which $P=(\mathrm{Max}(F_o^2, 0) + 2F_c^2)/3$; largest diffraction peak and hole: 0.39 and -0.59 e $Å^{-3}$. CCDC-698597 contains the supplementary crystallographic data for this paper. These data can be obtained free of charge from the Cambridge Crystallographic Data Center via www.ccdc.cam.ac.uk/data_request/cif.

Acknowledgements

This work was supported through a grant from the Ministry of Science and Higher Education (Project N204 074 32/2022). X-ray single-crystal measurements were taken at the Structural Research Laboratory (SRL), Chemistry Department, Warsaw University, Poland. The SRL has been established with financial support from European Regional Development Found in the Sectoral Operational Programme "Improvement of the Competitiveness of Enterprises, years 2004–2006", project no: WKP_1/1.4.3./1/2004/72/72/165/2005/U.

[1] E. R. Kay, D. A. Leigh, F. Zerbetto, *Angew. Chem.* **2007**, *119*, 72–196; *Angew. Chem. Int. Ed.* **2007**, *46*, 72–191; and references therein.
[2] S. Bonnet, J.-P. Collin, M. Koizumi, P. Mobian, J.-P. Sauvage, *Adv. Mater.* **2006**, *18*, 1239–1250; and references therein.
[3] J. Berna, D. A. Leigh, M. Lubomska, S. M. Mendoza, E. M. Perez, P. Rudolf, G. Teobaldi, F. Zerbetto, *Nature materials* **2005**, *4*, 704–710.
[4] A. Wieckowska, A. B. Braunschweig, I. Willner, *Chem. Commun.* **2007**, 3918–3920.
[5] E. Katz, O. Lioubashevsky, I. Willner, *J. Am. Chem. Soc.* **2004**, *126*, 15520.
[6] H.-R. Tseng, D. M. Wu, N. X. L. Fang, X. Zhang, J. F. Stoddart, *ChemPhysChem* **2004**, *5*, 111–116.
[7] B. C. Bunker, D. L. Huber, J. G. Kushmerick, T. Dunbar, M. Kelly, C. Matzke, J. Cao, J. O. Jeppsen, J. Perkins, A. H. Flood, J. F. Stoddart, *Langmuir* **2007**, *23*, 31–34.
[8] B. Korybut-Daszkiewicz, A. Wieckowska, R. Bilewicz, S. Domagała, K. Woźniak, *J. Am. Chem. Soc.* **2001**, *123*, 9356–9366.
[9] B. Korybut-Daszkiewicz, A. Wieckowska, R. Bilewicz, S. Domagała, K. Woźniak, *Angew. Chem.* **2004**, *116*, 1700–1704; *Angew. Chem. Int. Ed. Engl.* **2004**, *43*, 1668–1672.
[10] G. Bidan, M. Billon, B. Divisia-Blohon, J.-M. Kern, L. Raehm, J.-P. Sauvage, *New J. Chem.* **1998**, *22*, 1139–1149.
[11] L. Raehm, J.-M. Kern, J.-P. Sauvage, C. Hamann, S. Palacin, J. P. Bourgoin, *Chem. Eur. J.* **2002**, *8*, 2153–2162.
[12] A. Rybka, R. Koliński, J. Kowalski, R. Szmigielski, S. Domagała, K. Woźniak, A. Wieckowska, R. Bilewicz, B. Korybut-Daszkiewicz, *Eur. J. Inorg. Chem.* **2007**, 172–185.
[13] A. Wieckowska, M. Wisniewska, M. Chrzanowski, J. Kowalski, B. Korybut-Daszkiewicz, R. Bilewicz, *Pure Appl. Chem.* **2007**, *79*, 1077–1085.
[14] E. Laviron, *J. Electroanal. Chem.* **1979**, *101*, 19–28.
[15] H. Daifuku, K. Aoki, K. Tokuda, H. Matsuda, *J. Electroanal. Chem.* **1985**, *183*, 1–26.
[16] C. E. D. Chidsey, *Science* **1991**, *251*, 919–922; erratum: C. E. D. Chidsey, *Science* **1991**, *252*, 631.
[17] A. Ulman, *Chem. Rev.* **1996**, *96*, 1533–1554.
[18] H. Ju, D. Leech, *Phys. Chem. Chem. Phys.* **1999**, *1*, 1549–1554.
[19] S. Sêk, A. Misicka, R. Bilewicz, *J. Phys. Chem. B* **2000**, *104*, 5399–5402.
[20] S. Sek, R. Bilewicz, *J. Electroanal. Chem.* **2001**, *509*, 11–18.
[21] S. Sek, B. Palys, R. Bilewicz, *J. Phys. Chem. B* **2002**, *106*, 5907–5914.
[22] S. Sharma, G. J. E. Davidson, S. J. Loeb, *Chem. Commun.* **2008**, 582–584.
[23] E. Lestini, K. Nikitin, H. Müller-Bunz, D. Fitzmaurice, *Chem. Eur. J.* **2008**, *14*, 1095–1106.
[24] R. Bilewicz, B. Korybut-Daszkiewicz, A. Rogowska, J. Szydłowska, A. Wieckowska, S. Domagała, K. Woźniak, *Electroanalysis* **2005**,1463–1470.
[25] APEX2, Bruker, **2004**.
[26] G. M. Sheldrick, *Acta Crystallogr. Sect. A* **1990**, *46*, 467–473.
[27] G. M. Sheldrick, *Acta. Crystallogr. Sect. A* **2008**, *64*, 112–122.
[28] *International Tables for Crystallograph, Vol. C*, (Ed. A. J. C. Wilson), Kluwer, Dordrecht, **1992**.

Received: August 14, 2008
Published online: December 3, 2008

